Ab initio calculations of defects in Fe and dilute Fe-Cu alloys

C. Domain

EDF-R&D, EMA Les Renardières, F-77250 Moret sur Loing, France

C. S. Becquart

Laboratoire de Métallurgie Physique et Génie des Matériaux, USTL, CNRS UMR 8517,
Bât. C6, F-59655 Villeneuve d'Ascq Cedex, France

Point defects in Fe and dilute FeCu alloys are investigated by *ab initio* calculations based on density functional theory. The relaxed vacancy and interstitial and substitutional Cu atom formation energies are determined as well as some migration energies. The binding energies of various Cu containing defects believed to play an important role in the embrittlement of pressure vessel steels under radiation are calculated and discussed. The results are consistent with a Cu transport via a vacancy mechanism. The introduction of a Cu atom decreases the energy difference between the $\langle 110 \rangle$ dumbbell and the $\langle 111 \rangle$ dumbbell configurations, and should make the dumbbell rotation motion easier. The *ab initio* results are compared to the figures obtained with empirical interatomic potentials. The convergence of the results with the simulated system size is examined.

I. INTRODUCTION

Point defects (vacancies and interstitials) directly affect the kinetics and thermodynamics of metals and intermetallic alloys and it is thus very important to develop a good understanding of their properties, i.e., their structure and mobility, as well as the interactions they can have with impurities. In the case of radiation damage studies, knowledge of point defect properties is a crucial issue, not always available through experimental means. For instance, the displacement cascades induced by the interaction of neutrons with matter result in the formation of many vacancies and interstitials, the evolution of which affects the mechanical properties of the materials. Furthermore, radiation damage has been studied using atomic scale simulations (molecular dynamics and Monte Carlo methods) with empirical interatomic potentials for a long time; however the results are greatly affected by the potential used in the calculations,[1] and it is necessary to validate the potentials, in particular the point defect properties they predict.

However, experimental data on point defects are scarce even for Fe which has been extensively studied because of its technological importance. Indeed it is not so easy to experimentally determine precisely atomic quantities such as the formation energy of a single vacancy or that of an interstitial. Furthermore, these quantities are affected by the local environment (for instance, the impurities) of the defect which is very difficult to probe. The controversy over the vacancy migration energy in Fe (see results on the monovacancy below) is a typical example of the influence of environment and the role of impurities. *Ab initio* calculations have therefore an important role to play. The *ab initio* point defect calculations have been mostly dedicated to the study of the vacancy in pure elements, mainly nonmagnetic. To our knowledge, there have been almost no *ab initio* calculations of the vacancy migration energy or the interstitial formation energies, for which accurate atomic relaxations are essential.

Only a few *ab initio* studies have been devoted to the effect of interstitial impurities; see, for instance, the study of Mo in Yb metal[2] or Fe in hcp metals.[3]

In the nuclear industry, pressure vessel steel contains several elements; among them copper seems to play a key role in embrittlement under irradiation. In this context, FeCu alloys are studied experimentally as well as by computer simulations as model alloys.

We present in this work results obtained for the relaxed formation, migration, and binding energies of various defects, presumed to play an important role in the embrittlement of power reactor steels. Because point defects induce large lattice strain, the precise computation of the formation energies necessitates large supercells. Despite the increase in computational power, it is still very difficult to simulate by *ab initio* supercells containing more than a few hundred atoms.

The *ab initio* calculations were performed using two different methods (see computational procedures) which combination allows us to give a good estimate of the fully converged property despite limitations of the supercell size. We have also used molecular statics and semiempirical potentials designed to simulate FeCu alloys with supercells of different sizes (up to a few thousand atoms) to assess the convergence of the calculations with supercell size.

For some defects, the influence of the supercell relaxation—full relaxation as opposed to constant volume or ionic relaxation—is examined.

The paper is organized as follows: First, we present and discuss briefly the relative phase stabilities in pure Fe and pure Cu. We then examine the structure and energetics of simple point defects in Fe and calculate the substitutional energy and the migration energy of a single Cu atom in Fe. We then calculate some binding energies which appear to play a crucial role in the formation of the Cu precipitates and the Cu-rich objects observed to form under neutron radiation in FeCu alloys as well as in pressure vessel steels.[4,5]

　　　　　65 024103-1

II. METHODOLOGY

A. *Ab initio* calculations

Ab initio calculations based on density functional theory[6] (DFT) have now demonstrated their capability to treat enough atoms for investigating a large field in materials science.[7] Our calculations have been performed using the Vienna *ab initio simulation package* VASP.[8–10] The calculations were performed in a plane-wave basis, using fully non-local Vanderbilt-type ultrasoft pseudopotentials to describe the electron-ion interaction.[11] Exchange and correlation were described by the Perdew-Zunger functional,[12] adding a non-local correction in the form of the generalized gradient approximation (GGA) of Perdew and Wang.[13] All the calculations except when mentioned in the text were done in the GGA. The pseudopotentials were taken from the VASP library. For Fe, six $3d$ electrons are considered as valence ones together with two $4s$ (the reference state is more precisely $3d^{6.2}4s^{1.8}$). For Cu, 11 valence electrons are used: one $4s$ and ten $3d$ (reference $4s^1 3d^{10}$). The energy cutoff for the plane-wave basis set used throughout this work was 350 eV for atomic and cell relaxation calculation and 240 eV for relaxation of the atomic position at constant volume. The supercell approach with periodic boundary conditions (PBC's) was used to simulate point defects as well as pure phases. Brillouin zone (BZ) sampling was performed using the Monkhorst-Pack scheme.[14] For the pure element calculations, where small supercells can be used, the convergence within 1 meV per atom with respect to the discrete BZ sampling was achieved using a k point density around $6000 V_a$ where V_a is the Fe atomic volume. Forces were computed using the method derived by Feynman.[15] Volume and ions relaxations were performed using the standard conjugate-gradient algorithms implemented in the VASP code. During the relaxation runs, the BZ integration was achieved using a Methfessel-Paxton smearing of $\sigma = 0.2$ eV,[16] and once the relaxation was completed, accurate total-energy calculations were performed without smearing using the tetrahedron method.[17] In order to calculate local quantities such as the local density of states or the local magnetic moment, it is necessary to introduce atomic radii to proceed to local projections on some orbitals (s, p, and d). The values adopted throughout this work are the recommended ones, 1.302 and 1.312 Å for Fe and Cu, which correspond approximately to their atomic radii. The defect calculations were also performed at constant volume, thus relaxing only the atomic position in a supercell dimensioned with the equilibrium lattice parameter for Fe. This allows one to use a smaller plane-wave cutoff radius of 240 eV. These calculations will be later referred to as the constant volume relaxation. We checked that the error induced by this lower cutoff radius is negligible. For instance, we found it to be around 5 meV for the binding energies calculated with supercells containing 54 atoms. In all the results presented here, the number of k points is the total number of k points (not the number of irreducible k points). We will show that relaxation at constant volume can be achieved with a poor k point density without affecting the energies very much.

B. Calculations with semiempirical potentials

To calculate bulk properties such as the cohesive energy, the bulk modulus, and so on, one typically uses PBC's. However, when one wants to determine defect properties (and compare them to experimental data), the problem is more complicated. The use of PBC's implies that the calculation will give the formation energy of a density of interacting defects instead of that of one single defect, as the strain field created by the defect in its supercell will possibly interact with its image strain fields. This self-interaction should be weak for defects which do not perturb the crystal too strongly. This should be the case when replacing one atom by another atom with similar atomic radius, i.e., an Fe substitution by a Cu atom; to a lesser extent, it should also be the case for vacancies which strain fields are isotropic in most cases. However, for self-interstitials, which induce strong local distortions of the crystal, the strain field interactions may be more important. To avoid such a problem, very large supercells containing a few thousand atoms should be used. However, at the present time, even the most powerful computers cannot handle *ab initio* calculations in such large supercells. This is particularly true if magnetism is taken into account in the calculations.

In order to examine the influence of the supercell size on the energy convergence, the defect energies were also determined using a semiempirical interatomic potential and the classical molecular dynamics code DYMOKA.[18] Semiempirical interatomic potentials enable one to simulate very large supercells (up to a few 10^6 atoms) for which the formation or binding energies are fully converged with the system size. The casual embedded atom method (EAM) interatomic potential developed by Ludwig *et al.*[19] was used as a cohesive model for Fe and FeCu. This potential has been characterized in detail.[20] The vacancy and interstitial formation energies, as well as the vacancy and Cu migration energy in α-Fe, were determined as a function of the supercell size using an energy minimization method algorithm called quench molecular dynamics (QMD).[21]

In all the tables presented below, the ''number of atoms'' is more precisely the number of sites in the perfect supercell.

C. Bulk moduli calculations

Elastic properties are very sensitive to the choice of data points and the equation of state used in the fit of the energy-volume curve. To obtain the bulk modulus B, small isostatic compressions were applied to small supercells. The applied strains ε have to be high enough to minimize the error, but low enough so as to remain in the elastic regime. The strains in our calculations were no larger than a few tenths of a percent (0.4% or 0.5%). The bulk modulus B is then given by

$$B = \frac{1}{9\Omega_0} \frac{\partial^2 E_{tot}}{\partial^2 \varepsilon},$$

where Ω_0 is the atomic volume. In practice, we calculated the total energy E_{tot} for 10–20 values of the strain and fit the total-energy versus strain curve to a second-order polynomial.

D. Defect formation volume calculations

To calculate the defect formation volume, Kanzaki forces were used,[22] except when indicated in the text. Kanzaki forces are forces that when applied to a perfect harmonic lattice produce the same displacements that the defect does. They thus, to a first approximation, represent the forces with which the defect interacts with its neighboring atoms. We followed the procedure derived by Simonelli *et al.*[23] The calculation procedure is as follows: once the lattice has been fully relaxed, the defect (the two atoms forming the dumbbell or the vacancy) is removed from the supercell and an Fe atom is introduced in the central position (i.e., in the perfect lattice site). A region (hereby called region I) around that central atom is defined: it is the core region where the anharmonic behavior occurs. In this region, the atoms are restored to their original position. A second region (which contains the harmonic displacements) is defined, small enough so as not to include the defect self-interactions from the image supercell and large enough so that the forces on the atoms outside that region can be neglected and the dipolar tensor is converged. In what follows, region II contains both region I and the "harmonic" region. The forces on all the atoms belonging to region II are then calculated: these are the Kanzaki forces.

The dipolar tensor P is obtained from these forces: $P^{\alpha\beta} = \Sigma R_j^\alpha K_j^\beta$ with j in region II where K_j^β is the Kanzaki force on atom j in the β direction and R_j^α is the αth component of the vector joining atom j and the central atom. The defect relaxation volume is given by the trace of the dipolar tensor: $\Delta V = \mathrm{Tr}(P)/3B$, where B is the bulk modulus.[27] The vacancy formation volume Ω_v^f is given by $\Omega_v^f = \Delta V + \Omega_0$, where Ω_0 is the atomic volume of the perfect lattice. The interstitial formation volume Ω_i^f is given by $\Omega_i^f = \Delta V - \Omega_0$.

III. RESULTS

A. Fe structure

Fe, because of its technological importance, has been studied extensively, and its phase diagram under atmospheric pressure is well known. Fe crystallizes into a ferromagnetic body-centered-cubic (bcc) structure α-Fe at ambient temperature; the α phase transforms into a face-centered-cubic (fcc) phase γ-Fe above 1200 K, then to another bcc phase δ-Fe above 1700 K. Experimental work has shown that a bcc to hexagonal-close-packed (hcp) transition takes place at pressures of 10–15 GPa at room temperature.[24] Under extreme conditions (high temperatures and high pressures), another phase can be stabilized, which structure is still debated: double hcp[25] or orthorhombic.[26] The stability of the different phases versus volume (and thus strain) is beyond the scope of this work, and we have just examined the most stable configurations or some configurations found in the literature for each structure: bcc, fcc, and hcp, taking into account magnetism.

At 0 K, our calculations predict the ground state of Fe to be magnetic bcc as is observed experimentally [$T_{Curie} = 1043$ K (Ref. 28)]. However, as observed by Kresse and Joubert,[29] the magnetization is overestimated by $0.1\mu_B$/atom compared to the experimental results.[28]

γ-Fe can be stabilized by precipitation in a Cu matrix or by epitaxial growth on Cu substrates. It has been investigated intensively because of its complex magnetic structure and the well known Invar effect. Kraft *et al.* [using the linear muffin tin orbital (LMTO) in the local spin density approximation (LSDA)] found that when fcc Fe is constrained to the Cu lattice constant in the (001) plane and remains cubic, growth in the antiferromagnetic (AFM) phase is expected.[30] Häglund using LMTO methods and the fixed-spin-moment (FSM) procedure observed that both the GGA and the LSDA predict the existence of two ferromagnetic (FM) states.[31] The LSDA, however, favors the nonmagnetic (NM) state, while the GGA predicts the high-spin (HS) state to be the most stable. Krasko, using the Stoner model for itinerant ferromagnetism in combination with non-spin-polarized LMTO, found three different ferromagnetic states stable at the same volume,[32] but additional calculations showed that they were unstable with respect to tetragonal shear deformations.[33] Experiments have shown that the γ-Fe ground state most likely consists of a noncollinear, spiral magnetic structure,[34,35] this being confirmed by Uhl *et al.*[36] and Körling and co-workers,[37] using the LMTO in the atomic sphere approximation (ASA), but we cannot with the VASP code explore such configurations. We have thus calculated the energetics of the two AFM states [antiferromagnetic double-layer (AFMD) and the more common AFM-I with alternating layers of up and down spins] chosen by Herper *et al.* as being representative of the magnetic space.[38] The GGA predicts that the AFMD is the most stable and that both ferromagnetic phases have tetragonal structures. Our results compare well with other author's results. Herper and co-workers, using full potential linear augmented-plane-wave method (FP-LAPW) within the GGA also find that the AFM structure is the most stable; however, they cannot distinguish between both AFM phases.[38] By using pulsed laser deposition to produce isotropic AFM fcc Fe on Cu (111) films to their structural perfection, Shen *et al.* measured a magnetic moment of more than 2 μ_B. The values obtained in the GGA agree very well with these experimental findings.[39]

Our calculations predict that the most stable hcp structure is ferromagnetic. This is in contrast with the FP-LMTO work of Yoo *et al.* which predicts that it should be nonmagnetic.[40]

The data for pure Fe at 0 K are summarized Table I. All the energies are given relative to the most stable structure energy, i.e., the energy of the magnetic α-Fe phase (5.153 eV).

B. Cu structure

Cu is a noble metal. It crystallizes under a nonmagnetic fcc structure at ambient temperature. Table II presents the results obtained in the GGA as well as in the LDA. In the GGA the lattice parameter is overestimated by 10%, while it is underestimated by only 2% in the LDA.

In the first stages of precipitation of Cu in Fe, the Cu precipitates are coherent with the matrix and therefore have a bcc structure.[43] We have for this reason studied the stability

TABLE I. Relative total energies (eV), bulk modulus (GPa), and magnetic moment (μ_B/atom) for different structures of Fe [magnetic (M), nonmagnetic (NM), low spin (LS), high spin (HS), antiferromagnetic (AFM), common AFM (AFM-I), and AFM double-layer (AFMD)].

	Volume (Å^3)	ΔE_{coh} (eV/at.)	B (GPa)	μ (μ_B/at.)
		α-Fe		
	11.65	0	160	2.32
Expt. [a]	11.70	–	168	2.22
		γ-Fe		
NM	10.37	0.255	280	
NM FPLAW [b]	10.34		287	
NM PP-GGA [c]			246	
HS	12.26	0.122	155	2.63
HS LMTO-FSM [d]				2.61
HS FPLAW [b]	12.03	0.154	168	2.57
HS expt. [e]	12.11±0.04			
LS	10.89	0.222	f	1.36
LS FPLAW [b]	10.62		207	1.02
AFMD	11.63	0.098	145	±2.32
AFMD FPLAW [b]	11.02	0.101	125	1.80
AFM-I	11.11	0.147	180	±1.83
AFM-I FPLAW [b]	10.69	0.101	190	1.30
AFM expt. [e]	11.30±0.04			
AFM expt. [g]				0.7
		hcp		
M	12.36	0.166		2.60
NM	10.31	0.18		

[a]Reference 28.
[b]Reference 38.
[c]Reference 42.
[d]Reference 31.
[e]Reference 41, obtained by extrapolating 4 K experimental data about Fe fcc alloys.
[f]It was not possible to determine precisely the LS bulk modulus because of a phase transformation that took place.
[g]Reference 34.

TABLE II. fcc Cu cohesive energy (eV) and bulk modulus (GPa).

	Volume (Å^3)	E_{coh} (eV/atom)	B (GPa)
GGA	12.07	3.763	140
LDA	11.01	4.753	190
Expt. [a]	11.66	3.49	137

[a]Reference 28.

C. Defects structure in α-Fe

1. Monovacancy

The monovacancy formation energy (Tables IV and V) has been determined for supercells as large as 128 atoms (the values were not corrected for the residual pressure). The vacancy formation volume for the fully relaxed calculations (Table IV) was obtained by subtracting $(N-1)\Omega_0$ to the volume of the supercell, V, where Ω_0 is the atomic volume of the perfect lattice and N the number of atoms in the supercell. The energy obtained by VASP is in good agreement with the experimental data available. It appears that all the calculations (EAM, fully relaxed or constant volume) converge quickly with the supercell size. Figure 1 displays the evolution of the monovacancy formation energy versus supercell size for (a) the EAM potential and (b) the constant volume simulations. As can be seen, the energy converges rather quickly and is almost converged with 53 atoms. Furthermore, with 53 atoms and only one k point, the atom positions are almost correct. Indeed, for a 53-atom supercell, we determined the relaxed configurations obtained with 1 single k point and that obtained with 125 k points. We then calculated, using 125 k points, the energy of both configurations and found that the energy difference is only 2%. This amount is small compared to the energy change due to relaxation which represents 15% of the formation energy. With the 8-k-point relaxed configuration (instead of 1 single k point), the energy difference is 0.04%.

The dipolar tensor eigenvalues depend on the size of region II (see above) as can be seen Fig. 2; however, a value of 5.5 Å give converged results. Table V displays the vacancy formation energy and the vacancy formation volume obtained with this radius for the constant volume calculations. The results are very similar to those of the fully relaxed calculations.

The relaxation of the nearest-neighbor shells is isotropic (Table VI) and very important for the first three shells in contrast with group-V transition metals or group-VI transition metals.[48] This leads to a substantial energy difference between nonrelaxed and relaxed configurations as can be seen in Table IV.

Figure 3 displays the neighbor shell relaxations around the vacancy for the EAM calculations as well as for the constant volume ones. The relaxation oscillates: the first-neighbor shell relaxes towards the vacancy, the second outwards, the third inwards, etc. This is typical of body-centered structures.[54] The relaxation of the fourth-nearest-neighbor shell is close to 0.1% for the EAM calculations with 2000

of bcc Cu (Table III). The GGA and LDA predict a similar energy difference between the two Cu phases which appears to be underestimated as compared to the experimental results and to the full potential calculation of Kraft *et al.*[44] However, they both predict that the bcc phase lattice parameter is slightly larger than that of bcc Fe and therefore that a Cu precipitate small enough to remain in the bcc structure should induce compressive stresses in the lattice. This is indeed what is observed by Phythian *et al.* who estimate the lattice strain to be of the order of a few percent.[43] In agreement with Kraft *et al.*[44] and Lu *et al.*,[45] we did not find any stable body-centered-tetragonal phase.

TABLE III. Stability of bcc Cu: lattice parameter (Å), cohesive energy (eV/atom), bulk modulus (GPa), energy difference between the fcc and the bcc structure (eV/atom), and volume difference between the two structures (%).

bcc Cu	Volume (Å^3)	E_{coh} (eV/atom)	B (GPa)	$\Delta E_{fcc\text{-}bcc}$ (eV/atom)	$\dfrac{\Omega_{Cu_{fcc}}-\Omega_{Cu_{bcc}}}{\Omega_{Cu_{fcc}}}$	$\dfrac{\Omega_{Fe_{bcc}}-\Omega_{Cu_{bcc}}}{\Omega_{Fe_{bcc}}}$
GGA	12.12	3.727	160	0.036	-0.41%	-4.03%
LDA	11.06	4.712	180	0.041	-0.45%	-5.03%
FP-LMTO [a]				0.007	-4.3%	
LAPW [b]				0.049	-0.8%	
PP-GO [c]	11.82	3.81	185	0.02		
Expt. [d]	12.07				-3.5%	-3.2%

[a]Reference 44.
[b]Reference 45.
[c]Reference 46, PP-GO: pseudopotentials with local orbital basis consisting of Gaussians.
[d]Reference 47, the experimental result is the lattice parameter of bcc Cu precipitates found to form under electron irradiation with a fluence of 0.6 Ccm^{-2} at 300 °C in Fe 1.5 wt % Cu.

atoms. This indicates that a good estimate of the vacancy formation energy can be obtained using a supercell including up to the fifth or sixth neighbors. This is indeed the case by *ab initio* calculations: the formation energies obtained with a 54-atom supercell do not vary much from that obtained with the 128-atom supercell.

There has been some controversy about the experimental vacancy migration energy: for instance Schaefer *et al.*[49] found a value of 1.28 eV, while Vehanen *et al.* published a vacancy migration energy of 0.55 eV.[55] This data scattering

comes very likely from the difficulty to obtain very pure Fe crystals. Impurity atoms, even in very small amounts, trap the vacancies and thus decrease the vacancy diffusion coefficient. Indeed the much smaller value of 0.55 eV was measured for a high-purity α-Fe.[55]

The migration energy was calculated as follows. For the EAM potential, a static approach was used. A single Fe atom, nearest neighbor to the vacancy, is moved step by step along the $\frac{1}{2}\langle 111\rangle$ vector joining the two sites. After each move, the whole lattice is allowed to relax according to the QMD al-

TABLE IV. Vacancy formation energy (eV) and formation volume (per atomic volume) obtained by fully relaxed calculations. For the EAM potential the formation volume was obtained using Kanzaki forces with a radius of 5.5 Å for region II and restoring only the central atom to its initial position; i.e., region I contains only one atom. The value of the bulk modulus B is equal to 160 GPa for the *ab initio* calculations and to 180 GPa for the EAM calculations (as predicted by the interatomic potential from Ref. 1).

	E_{vac}^f (eV)	E nonrelaxed (eV)	E ion. relaxed (eV)	a (Å)	Ω_V^f/Ω_0
Fully rel. 16 atoms (1000 k points)	2.01	2.21		2.842	0.82
Fully rel. 27 atoms (216 k points)	1.93	2.24		2.846	0.81
Fully rel. 54 atoms (125 k points)	1.95	2.24	1.94 [a]	2.852	0.90
EAM potential 16000 atoms	1.63	1.79		2.867	0.82
LSGF [b]		2.25 [c]			0.55
FP-LMTO [d]	2.18				
Expt.	1.53, [e] 2 [f]				0.95 [g]

[a]The difference between the fully relaxed value and the ionic relaxed value falls in the error range expected from calculations with 54 atoms. This explains why the fully relaxed value appears to be slightly higher than the ionic relaxed energy.
[b]Reference 53.
[c]Data obtained with a locally self-consistent Green's function including electrostatic multipole corrections to the atomic sphere approximation. The effects of local lattice relaxations were neglected, but volume relaxation was taken into account. As our work shows that the local lattice relaxation contributes the most and by far to the energy decrease, we interpret Korzhavyi results (Ref. 53) as being nonrelaxed energies.
[d]Reference 48.
[e]Reference 49.
[f]Reference 50.
[g]Reference 51.

TABLE V. Vacancy formation energy (eV) and vacancy formation volume obtained with constant volume calculations with a lattice parameter $a = 2.854$ Å. The vacancy formation volume was obtained using Kanzaki forces with a radius of 5.5 Å for region II and restoring only the central atom to its initial position; i.e., region I contains only one atom. The value of the bulk modulus B is equal to 160 GPa for the *ab initio* calculations and to 180 GPa for the EAM calculations (as predicted by the interatomic potential from Ref. 1).

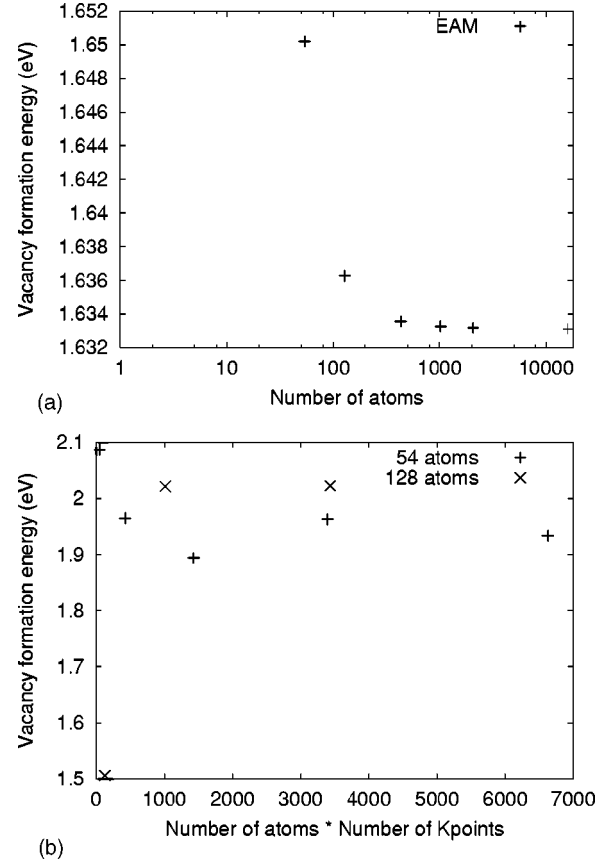|	E_{vac}^f (eV)	Ω_V^f/Ω_0
Const. vol. 16 atoms (216 k points)	2.05	
Const. vol. 16 atoms (343 k points)	2.05	
Const. vol. 54 atoms (1 k point)	2.09	
Const. vol. 54 atoms (8 k points)	1.96	
Const. vol. 54 atoms (27 k points)	1.89	
Const. vol. 54 atoms (64 k points)	1.96	
Const. vol. 54 atoms (125 k points)	1.93	0.64
Const. vol. 128 atoms (1 k point)	1.51	
Const. vol. 128 atoms (8 k points)	2.02	
Const. vol. 128 atoms (27 k points)	2.02	0.58
EAM potential 54 atoms	1.65	0.85
EAM potential 128 atoms	1.63	0.82
EAM potential 2000 atoms	1.63	0.82

(a)

(b)

FIG. 1. Vacancy formation energy vs supercell size: (a) semi-empirical EAM potential results and (b) VASP constant volume calculations with a 240 eV energy cutoff radius.

gorithm to find the minimum energy of the configuration. During the relaxation the coordinate of the "displaced" atom is fixed along [111] while the other two coordinates can relax in the (111) plane. The migration energy is then given by the height of the energy barrier (the saddle point). For the VASP calculations presented here, only the saddle point energy value was determined. The atom is positioned at the saddle point, the structure is relaxed using the conjugate gradient algorithm, and the energy is determined. The results are presented Table VII. The migration energy obtained by the constant volume calculations appears to be well converged with respect to the k point density and close to the experimental result for extremely pure Fe,[55] as well as to the results of the fully relaxed calculations.

2. Self-interstitials

In metals, the most stable interstitial defects are dumbbells: two atoms sharing one lattice site. We have calculated the relaxed formation energy of the three possible types of dumbbells. The relaxed ⟨111⟩ dumbbell configuration is more precisely a crowdion, i.e., four atoms sharing three lattice sites. The results are presented Table VIII. The convergence with the supercell size has also been examined and is displayed Figs. 4 and 5. It is unexpectedly fast, even for the ⟨111⟩ dumbbell. The most stable defect predicted by *ab initio* calculations is the dumbbell along ⟨110⟩, in agreement with experiments.[51] To our knowledge, no experimental values are available for the interstitial formation energies. It must be noticed that the EAM potential used in this work predicts the ⟨111⟩ crowdion to be the most stable. This prob-

lem has been discussed in the literature[52] and seems to be a consequence of the range of the many-body interatomic potential.

The energy difference between the ⟨110⟩ and the ⟨111⟩ dumbbell is important for the study of interstitial and interstitial cluster stability and diffusion. Indeed computer simulations show that the ⟨110⟩ dumbbell motion involves on-site rotation to the ⟨111⟩ dumbbell configuration.[57,58] The energy difference between the two configurations is thus important to determine the amount of time the dumbbell spends in each configuration even if it does not give all the information about the energy path the dumbbell has to follow to rotate (i.e., the saddle point). Table VIII shows that the EAM potential underestimates this value compared to the *ab initio* results. This is also the case for another shorter-range EAM potential which stabilizes the ⟨110⟩ dumbbell.[56] This general underestimation of the energy difference between the two dumbbell configurations could be a possible explanation for the difference observed between the experimental interstitial migration energy [0.3 eV (Ref. 27)] and the molecular dynamics determined interstitial migration energy [0.023 eV (Ref. 59)].

The constant volume value results appear to be systematically close to 0.5 eV larger than the fully relaxed data. This is not so surprising. In a large system, the subsystem corresponding to the simulated supercell is in equilibrium with the
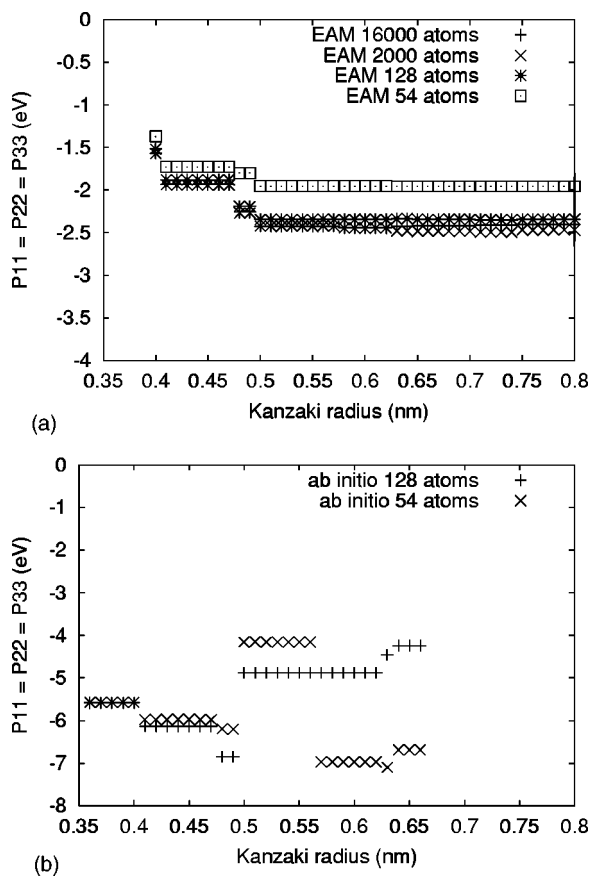
(a)

(b)

FIG. 2. Dipolar tensor eigenvalues for the vacancy obtained using the Kanzaki forces (see above) vs region II radius to calculate the Kanzaki forces (value of the bulk modulus *B* equal to 180 GPa for the EAM calculations and 160 GPa for the *ab initio* calculations): (a) semiempirical EAM potential results and (b) VASP constant volume calculations with a 240 eV energy cutoff radius.

(a)

(b)

FIG. 3. Nearest-neighbor shell relaxation around the vacancy (%): (a) semiempirical EAM potential results and (b) VASP constant volume calculations.

rest of the material and the presence of a defect results in a nonzero equilibrium pressure on the subsystem borders as well as some local atomic displacements, i.e., volume changes. In the fully relaxed simulations, the supercells undergo very large volume changes and some distortion to equilibrate the pressure to zero. Such volume changes and distortion would be partly impeded by the surrounding matter in a real material. In the constant volume calculations, however, no volume change and no cell distortion at all is allowed to take place.

In a bulk material, the volume of the subsystem represented by the supercell is therefore between the nonrelaxed volume and the fully relaxed volume. The two methods thus
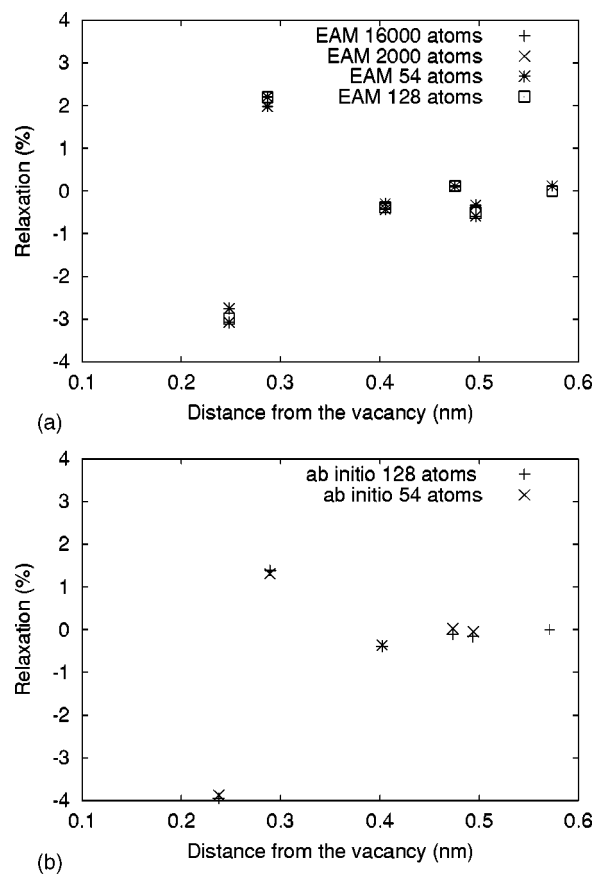
give the interval in which to find the *ab initio* value obtained for a supercell of infinite size (comparable to a real bulk material). For the vacancy, no distortion and only small volume changes (0.2% for a 54-atom supercell) are observed and the fully relaxed and constant volumes calculations give results very close to each other and to the experimental data. For the dumbbells, big distortions (for example, an angle of shear of 0.3° for the ⟨110⟩ dumbbell) and large volume changes (4.0% for a 54-atom supercell) take place in the fully relaxed calculations and the difference with the constant volume simulations are therefore more important. (It should be added that the shearing of the supercell has almost no effect on the energy of the system and can be neglected.) The formation energy of Frenkel pairs in Fe has been determined experimentally and found to be around 6.3, 6.6 eV.[60] The fully relaxed calculations predict a value of 1.93+3.41

TABLE VI. First fifth-neighbor shell relaxation (%) around the vacancy for the *ab initio* calculations.

	First neigh.	Second neigh.	Third neigh.	Fourth neigh.	Fifth neigh.
Fully rel. 27 atoms (216 *k* points)	−3.9%	+1.2%	−0.8%	−	−
Fully rel. 54 atoms (125 *k* points)	−4.02%	+1.38%	−0.36%	+0.05%	−0.06%
Const. vol. 54 atoms (125 *k* points)	−4%	+1.3%	−0.37%	+0.03%	−0.04%
Const. vol. 128 atoms (27 *k* points)	−3.9%	+1.4%	−0.39%	−0.10%	−0.16%

TABLE VII. Vacancy migration energies (in eV).

	$E_{vac}^{mig.}$ (eV)
Fully rel. 27 atoms (64 k points)	0.45
Fully rel. 54 atoms (125 k points)	0.65
Const. vol. 16 atoms (125 k points)	0.66
Const. vol. 54 atoms (125 k points)	0.64
Const. vol. 128 atoms (27 k points)	0.65
EAM potential 2000 atoms	0.67
Expt.[a]	0.55

[a]Reference 55.

$=5.34$ eV, while the constant volume ones predict a value of $2.02+3.94=5.96$ eV. The *ab initio* predictions are quite comparable to the experimental results for which no error estimate was found.

To gain some insight into the strain field induced by the defects and compare to experimental data, we calculated the dipolar tensor using Kanzaki forces.[22] For the interstitials, anharmonic effects extend over a large region, and to obtain converged results for the EAM potential, we had to include the fifth-neighbor shell in region I and use a radius of $11-12$ Å for region II, which makes the estimation of the dipolar tensor unrealistic for the *ab initio* calculations if one wants to compare them to the experimental data. Table IX thus presents the dipolar tensor eigenvalues, as well as the relaxation volumes which can be obtained from the dipolar tensor trace for the EAM potential only. We must add that the dipolar tensor eigenvalues from *ab initio* calculations can be very useful even if not close to the experimental results because of the limited supercell size, if one wants to build semiempirical potentials as they can be used as fitting parameters. However, this particular point is not the purpose of the present article. The distance between the two $\langle 110 \rangle$ dumb-
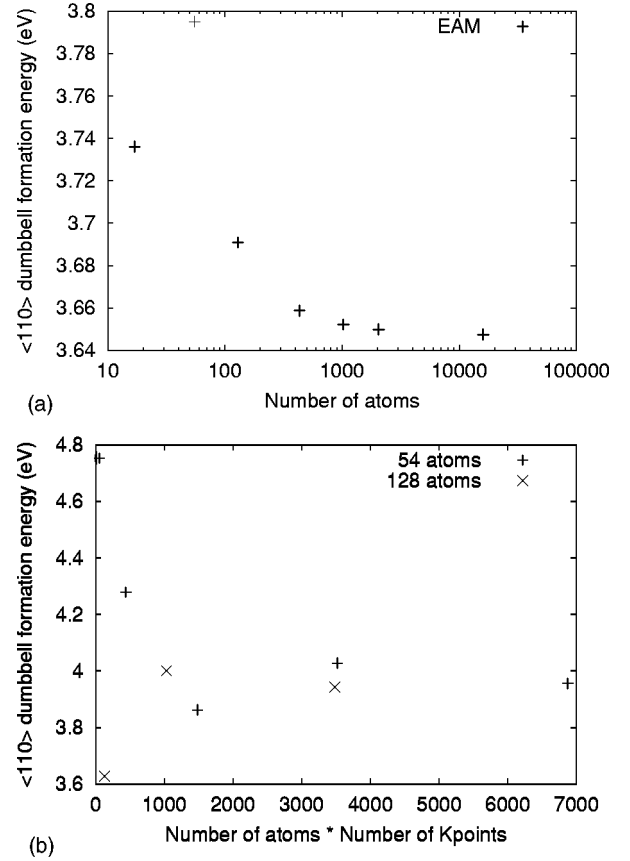

(a)

(b)

FIG. 4. Convergence of the $\langle 110 \rangle$ dumbbell formation energy vs supercell size: (a) semiempirical EAM potential results and (b) VASP constant volume calculations.

bell atoms is 1.905 Å for 54 atoms (64 k points), i.e., 0.771 nearest-neighbor unit.

The analysis of the local magnetic properties in the vicinity of the interstitial defects shows that the interstitial mag-

TABLE VIII. Self-interstitial defect formation energies (eV).

|	$E_{\langle 100 \rangle}^{f}$ (eV)	$E_{\langle 110 \rangle}^{f}$ (eV)	$E_{\langle 111 \rangle}^{f}$ (eV)	$\Delta E_{\langle 111 \rangle - \langle 110 \rangle}$ (eV)
Fully rel. 27 atoms (64 k points)	4.59	3.84	4.64	0.8
Fully rel. 54 atoms (27 k points)	4.28	3.37	4.06	0.69
Fully rel. 54 atoms (125 k points)	4.37	3.41	4.11	0.7
Const. vol. 54 atoms (1 k point)	5.57	4.75	5.13	0.38
Const. vol. 54 atoms (8 k points)	5.48	4.28	5.06	0.81
Const. vol. 54 atoms (27 k points)	4.99	3.86	4.67	0.81
Const. vol. 54 atoms (64 k points)	5.11	4.03	4.79	0.76
Const. vol. 54 atoms (125 k points)	5.07	3.96	4.75	0.79
Const. vol. 128 atoms (1 k point)	4.92	3.63	5.23	1.6
Const. vol. 128 atoms (8 k points)	5.08	4.00	4.71	0.71
Const. vol. 128 atoms (27 k points)	5.04	3.94	4.66	0.72
EAM potential 2000 atoms	4.57	3.67	3.54	-0.13
Short-range EAM potential[a]	–	4.87	5.00	0.13

[a]Reference 56.

(a)

(b)
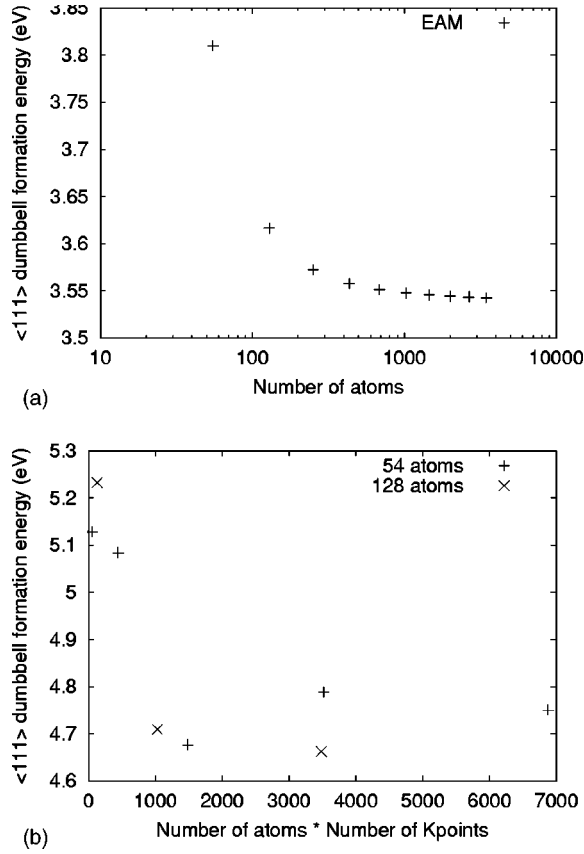
FIG. 5. Convergence of the $\langle 111 \rangle$ dumbbell formation energy vs supercell size: (a) semiempirical EAM potential results and (b) VASP constant volume calculations.

netic moment is reduced (Fig. 6). For the $\langle 110 \rangle$ dumbbell, the moment is even antiferromagnetic with respect to the rest of the crystal. The local moment on the dumbbell first neighbors is also slightly decreased. The results agree with the model of Ono and Mateta which predicts a decrease in the local magnetic moment of the interstitial atom and its neighbors because of the pressure from the surrounding atoms.[61]
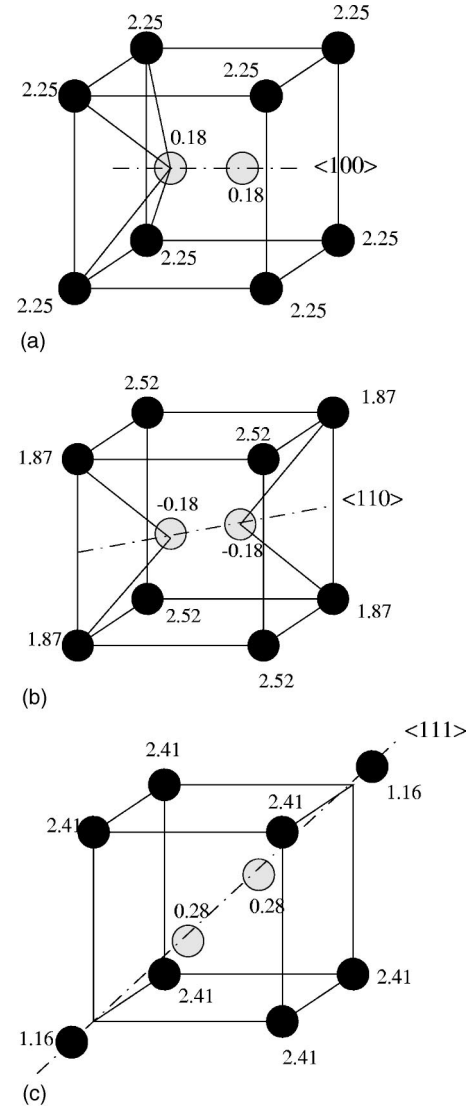

FIG. 6. Local magnetic moment on the interstitials and their neighbors (in μB): (a) $\langle 100 \rangle$ dumbbell, (b) $\langle 110 \rangle$ dumbbell, and (c) $\langle 111 \rangle$ dumbbell.

TABLE IX. Dipolar tensor eigenvalues (in eV) and formation volume (in atomic volumes) for the $\langle 110 \rangle$ and $\langle 111 \rangle$ dumbbells calculated using Kanzaki forces (constant volume calculations). The eigenvectors are $(110)(\bar{1}10)(001)$ for the $\langle 110 \rangle$ dumbbell and $(111)(\bar{1}10)(11\bar{2})$ for the $\langle 111 \rangle$ dumbbell. The formation volume and the dipolar tensor eigenvalues were obtained using Kanzaki forces (see above) with a radius of 12 Å for region II and including the fifth-neighbor shell in region I. The value of the bulk modulus B was taken equal to 180 GPa.

	E^f (eV)	P_1 (eV)	P_2 (eV)	P_3 (eV)	Ω_i^f/Ω_0
$\langle 110 \rangle$ EAM 2000 atoms	3.67	18.7	10.8	14.5	0.11
$\langle 110 \rangle$ EAM 16000 atoms	3.67	18.6	10.7	14.5	0.11
$\langle 110 \rangle$ Expt.[a]		17.3	7.3	16.4	0.1
$\langle 111 \rangle$ EAM 2000 atoms	3.54	23.3	11.2	11.2	0.15
$\langle 111 \rangle$ EAM 16000 atoms	3.54	23.3	11.2	11.2	0.15

[a]Reference 51.

TABLE X. Substitutional energy of Cu in Fe (in eV).

	E_{sub} (eV)	E nonrelaxed (eV)	a (Å)
Fully rel. 16 atoms (512 k points)	0.44		2.878
Fully rel. 27 atoms (216 k points)	0.55		2.871
Fully rel. 54 atoms (125 k points)	0.50	0.53	2.864
Const. vol. 16 atoms (343 k points)	0.52	0.53	2.854
Const. vol. 54 atoms (125 k points)	0.54		2.854
Const. vol. 128 atoms (27 k points)	0.55		2.854
EAM 16000 atoms	0.50	0.56	2.867
Expt.[a]	0.59		
CALPHAD[b]	0.412		

[a]Reference 62.
[b]Reference 63.

3. Substitutional Cu atom

We have computed the substitutional energy E_{sub} of a single Cu atom in an α-Fe matrix (Table X). E_{sub} is given by $[E(n\text{Fe}+1\text{Cu})_{bcc}-[n*E(\text{Fe})_{bcc}]-E(\text{Cu})_{fcc}]$ where $E(n\text{Fe}+1\text{Cu})_{bcc}$ is the energy of a supercell containing n Fe atoms and 1 Cu atom, $E(\text{Fe})_{bcc}$ is the cohesive energy of α-Fe, and $E(\text{Cu})_{fcc}$ is the cohesive energy of fcc Cu. The results appear to be converged with respect to the supercell size and agree very well with the experimental data. Here also, we observe a very quick convergence of the substitutional energy versus supercell size with the EAM potential.

Table XI displays the neighbor relaxation around the Cu atom. The relaxation of the fifth-neighbor shell is surprisingly high from what could be expected of the small size difference between the Cu atom and the Fe atom and could indicate a need for very large supercells for such calculations. This however does not seem to affect the substitutional energy as can be seen Table X. The neighbor shell relaxation in the *ab initio* calculations oscillates in a pattern similar to that of the vacancy (except that the signs are different; i.e., the first-neighbor shell relaxes outwards around the Cu atom, while it relaxes inwards around the vacancy). For the EAM potential, the relaxation scheme appears to be different.

TABLE XII. Migration energy of a single Cu atom in α-Fe (in eV).

	E_{Cu}^{mig} (eV)
Fully rel. 54 atoms (27 k points)	0.64
Fully rel. 54 atoms (125 k points)	0.53
Const. vol. 54 atoms (125 k points)	0.56
Const. vol. 128 atoms (27 k points)	0.55
EAM potential 2000 atoms	0.22

4. Migration energy of Cu in Fe

Table XII presents the migration energy of a single Cu atom in an α-Fe matrix. The procedure is similar to the one used to determine the vacancy migration energy except that the atom which is moved towards the vacancy is a Cu atom in the EAM, while in the VASP calculations, it is a Cu atom which is positioned at the saddle point.

In that case also, we checked that the energy convergence versus supercell size is similar to that of Fig. 4 or 5. For the *ab initio* calculations, the migration energy appears to be well converged at constant volume relaxation with respect to the k point density. The Cu migration energy is lower than the vacancy migration energy in agreement with the semiempirical potential results. No experimental data are available to compare to our results.

5. Divacancy, V-Cu, Cu-Cu, and dumbbell Cu binding energies

Computer simulations[20,64] have shown that small mixed-Cu objects form during or right after displacement cascades in FeCu alloys. The relative stability of these objects depends among other aspects on their binding energies, for which almost no experimental data can be found. We thus try in this work to determine some of these binding energies.

The binding energies between two entities in a bcc iron matrix are calculated as follows. The binding energy $E_b(AB)$ is defined as the difference of the two system energies E_1 and E_2, system 1 where A and B do not interact and system 2 where A and B interact. The distance between A and B may be the first-nearest-neighbor distance, second-nearest distance, and so on. The binding energy $E_b(AB)$ is the differ-

TABLE XI. First fifth-neighbor shell relaxation (%) around the Cu atom.

	First neigh.	Second neigh.	Third neigh.	Fourth neigh.	Fifth neigh.
Fully rel. 27 atoms (216 k points)	+0.4%	−0.04%	0.0%	−	−
Fully rel. 54 atoms (125 k points)	+1.18%	−0.38%	+0.11%	−0.20%	+0.34%
Const. vol. 54 atoms (125 k points)	+0.92%	−0.23%	+0.13%	−0.20%	+0.34%
Const. vol. 128 atoms (27 k points)	+0.93%	−0.13%	+0.05%	−0.04%	+0.28%
EAM potential 54 atoms	+0.91%	+1.03%	−0.13%	+0.09%	+0.18%
EAM potential 128 atoms	+0.92%	+1.13%	−0.10%	+0.14%	+0.17%
EAM potential 2000 atoms	+0.95%	+1.15%	−0.08%	+0.16%	+0.19%
EAM potential 16000 atoms	+0.94%	+1.15%	−0.08%	+0.16%	+0.19%

TABLE XIII. Relaxed binding energies (E_b) (in eV) for the divacancy, V-Cu, and Cu-Cu in the α-Fe matrix obtained by method I.

	V-V		V-Cu		Cu-Cu	
	First neigh. (eV)	Second neigh. (eV)	First neigh. (eV)	Second neigh. (eV)	First neigh. (eV)	Second neigh. (eV)
Fully rel. 54 atoms (125 k points)	0.06	0.15	0.11	0.10	0.17	0.09
Const. vol. 54 atoms (64 k points)	0.01	0.11	0.05	0.10	0.18	0.07
Const. vol. 54 atoms (125 k points)	0.01	0.11	0.05	0.09	0.18	0.07
Const. vol. 128 atoms (8 k points)	0.14	0.28	0.17	0.18	0.16	0.04
Const. vol. 128 atoms (27 k points)	0.15	0.29	0.16	0.18	0.14	0.03
EAM potential 4000 atoms	0.16	0.21	0.19	−0.03	0.2	−0.02

ence between the two system total energies $E_b(AB)=E_1-E_2$.

The relaxed binding energies obtained with this procedure are given Table XIII for the divacancy, the V-Cu, and the Cu-Cu systems. The calculations predict that the most stable relaxed configurations are the first nearest neighbors for the Cu-Cu and the Cu-V system and the second nearest neighbors for the V-V system. The divacancy binding energy is an important parameter for the formation of vacancy clusters and voids. Unfortunately, no experimental data are available to compare to. Masuda investigated the properties of vacancy-type lattice defects in bcc transition metals using a tight-binding-type electronic theory.[65] His results show that the most stable relaxed configuration for the divacancy in transition metals is when the vacancies are second nearest neighbors. This is also observed experimentally in Mo.[66] Our results agree with this observation.

The experimental value for the V-Cu binding energy is 0.14 eV (Ref. 67) or 0.11 eV (Ref. 68); however, the relative positions of the Cu and the V are unknown. Our results lie in that experimental range. The strong first-neighbor Cu-V binding energy combined with the low value of the Cu migration energy is consistent with Cu transport by a vacancy diffusion mechanism, as is observed in kinetic Monte Carlo simulations.[64]

The defects studied in that paragraph are bigger and induce larger strain fields and distortions than the monovacancy or the substitutional Cu atom, hence the bigger difference between the fully relaxed and constant volume simulations. Furthermore, the values determined here are small and the relative errors are therefore more important.

Because of the relatively small supercell sizes one may use, it is rather difficult to make sure that the two entities in system 1 do not interact even when they are as far as the supercell size allows. Another method can be used to determine the binding energies which consists in subtracting the energy of system 2 (where A and B interact), the energy of a system containing A (calculated with a supercell with a size similar to that of system 2), as well as that of a system containing B (obtained with similar conditions) and that of the supercell with neither A nor B. The binding energy obtained with this approach will be referred to as the indirect binding energy $E_b^{indirect}(AB)$. For a supercell containing N atoms, it is obtained as $E_b^{indirect}(AB)=E(N-2+A+B)-E(N-1+A)-E(N-1+B)-E(N)$, where $E(N)$ is the energy of the supercell without A and B, $E(N-1+A)$ [$E(N-1+B)$] is the energy of the supercell with A [B] and $E(N-2+A+B)$ is the energy of the cell containing both A and B, i.e., the energy of system 2 in the previous method. If

TABLE XIV. Relaxed binding energies (in eV) for the divacancy, V-Cu, and Cu-Cu in the α-Fe matrix obtained with the two methods described above. The number of atoms in the first row is the number of atoms in the perfect supercell. The calculations were done at constant volume.

	Fully rel. E_b (eV)	54 atoms $E_b^{indirect}$ (eV)	Const. vol. E_b (eV)	54 atoms $E_b^{indirect}$ (eV)	Const. vol. E_b (eV)	128 atoms $E_b^{indirect}$ (eV)
V-Cu first neigh.	0.11	0.14	0.05	0.17	0.16	0.17
V-Cu second neigh.	0.10	0.20	0.09	0.21	0.18	0.19
V-Cu noninteracting	0 by def.	0.09	0 by def.	0.12	0 by def.	0.01
Cu-Cu first neigh.	0.17	0.17	0.18	0.15	0.14	0.14
Cu-Cu second neigh.	0.09	0.09	0.07	0.04	0.03	0.03
Cu-Cu noninteracting	0 by def.	−0.01	0 by def.	0.03	0 by def.	0.01
V-V first neigh.	0.06	0.14	0.02	0.10	0.15	0.15
V-V second neigh.	0.15	0.23	0.11	0.20	0.29	0.29
V-V noninteracting	0 by def.	0.08	0 by def.	0.09	0 by def.	−0.01

TABLE XV. Relaxed binding energies E_b (in eV) for Cu $\langle 110 \rangle$ and $\langle 111 \rangle$ dumbbells in the α-Fe matrix obtained by method I.

	E_b (eV)		
	$\langle 110 \rangle$ dumb. Cu inside	$\langle 110 \rangle$ dumb. Cu first neighbor	$\langle 111 \rangle$ dumb. Cu inside
54 atoms fully rel. (125 k points)	-0.22	$+0.16$	$+0.2$
Const. vol. 128 atoms (8 k points)	-0.36	$+0.11$	$+0.17$
Const. vol. 128 atoms (27 k points)	-0.43	$+0.10$	$+0.13$

the system is large enough, both methods should lead to the same result. Table XIV compares the results obtained by the two methods described above. With 128-atom supercells, similar binding energies are obtained, thus giving us confidence that the energy calculations are converged with respect to the supercell size.

For the binding energy of Cu with dumbbells, we found that, as can be seen in Table XV, the Cu atom prefers to be first-neighbor to the $\langle 110 \rangle$ dumbbell [Fig. 7(a)] or part of the $\langle 111 \rangle$ dumbbell (Fig. 7). The second method confirms the trends of Table XV. The Cu-$\langle 110 \rangle$ binding energy is found to be of the same order of magnitude as the Cu-V binding energy. Maury and co-workers[69] found a weak but positive binding between solute and interstitial atoms in FeCu. They observed that mixed dumbbells form at low temperatures (20 K), which, however, are not stable above 100 K. To examine this particular point, we ran molecular dynamics simulations with two semiempirical potentials found in the literature[56,19] for 150 p at 300 and 800 K. The starting configuration was a mixed dumbbell in a pure Fe lattice. After a few steps, the dumbbell released the Cu atom and traveled (as a pure Fe dumbbell) in the array. The Cu atom thus remained in the neighborhood of its initial position and was not transported anywhere. Interstitials may nevertheless still play a role in Cu atom transport. The *ab initio* results show that the presence of a Cu atom in the $\langle 110 \rangle$ dumbbell increases its energy while for the $\langle 111 \rangle$ dumbbell the opposite is observed (Table XV). The energy difference between the $\langle 110 \rangle$ and the $\langle 111 \rangle$ configurations is therefore decreased in the presence of a Cu atom and it is thus easier to go from one configuration to another. These results agree with these of Marian *et al.* who studied by semiempirical molecular dynamics the effect of Cu on self-interstitials and interstitial cluster migration.[70] They used the EAM potential derived by Ackland and co-workers[56] and observed that Cu solute atoms enhance the dumbbell rotation.

IV. CONCLUSIONS

We have calculated using an *ab initio* approach (VASP code) the properties of point defects in pure Fe as well as FeCu dilute alloys. The pure element ground states as well as some of their other typical structures agree with known experimental results. The calculations predict a relaxed vacancy formation energy around 1.9 eV and a vacancy migration energy around 0.65 eV. They also predict the $\langle 110 \rangle$ dumbbell as the most stable dumbbell with a relaxed forma-

tion energy between 4.4 and 5 eV. These values are globally consistent with the experimental results and demonstrate the ability of *ab initio* calculations as predictive tools for studying point defects.

The 0.7 eV energy difference between the $\langle 110 \rangle$ and $\langle 111 \rangle$ configuration is larger than the value typically obtained with empirical potentials. This could explain the discrepancy between the experimental dumbbell mobility and that obtained in MD simulations.

The substitutional energy of a Cu atom is found to be around 0.50 eV. The Cu migration energy in pure Fe is predicted to be lower than the vacancy migration energy. The binding energies of defects believed to play an important role in the embrittlement of pressure vessel steel under radiation are in agreement with the experimental data, when available. The strong Cu-V binding energy combined with the lower Cu migration energy is consistent with a Cu transport mechanism through vacancies. It is also found that the presence of
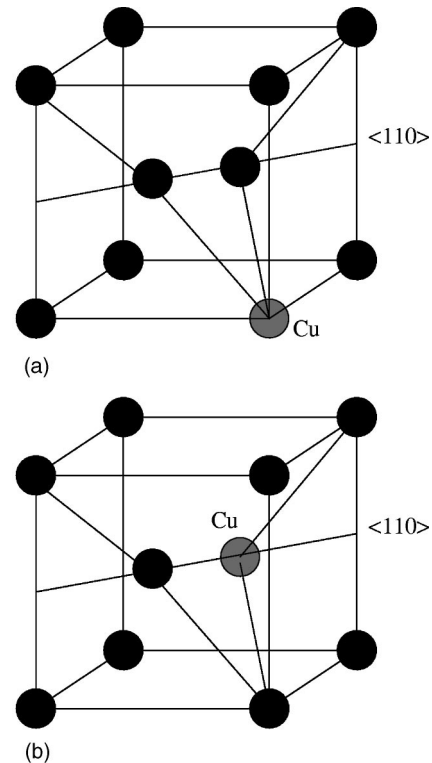

FIG. 7. Schematic drawing of (a) Cu atom first neighbor to the $\langle 110 \rangle$ dumbbell and (b) Cu atom inside the $\langle 110 \rangle$ dumbbell.

a Cu atom decreases the energy difference between the $\langle 110 \rangle$ dumbbell and $\langle 111 \rangle$ dumbbell configurations, thus making the dumbbell rotation easier.

These defects calculations were done using two different methods which combination allows to obtain a good estimate of the property to be determined despite the limitations of the supercell sizes. We examined in details the convergence of the calculations with the supercell size as well as with the number of k points and found that it was rather fast and that a good deal of information could be obtained with reduced numbers of k points.

Ab initio point defect characterization contributes thus to understand the elementary phenomena at the source of metal kinetics. All these data can also be used to build empirical potentials or as input parameters in higher-scale models and simulations. They can be used to check the validity of existing semiempirical potentials. In that sense, we found that the EAM potential predictions were not very far from the *ab initio* calculations. The effect of other solute elements and impurities is under study.

[1] C.S. Becquart, C. Domain, A. Legris, and J.C. van Duysen, J. Nucl. Mater. **280**, 73 (2000).

[2] A.A. Tulapurkar, S.N. Mishra, R.G. Pillay, H.G. Salunke, G.P. Das, and S. Cottenier, Phys. Rev. Lett. **85**, 1978 (2000).

[3] S. Frota-Pessôa, L.A. de Mello, H.M. Petrilli, and A.B. Klautau, Phys. Rev. Lett. **71**, 4206 (1993).

[4] M. Akamatsu, J.C. van Duysen, P. Pareige, and P. Auger, J. Nucl. Mater. **225**, 225 (1995).

[5] M. Akamatsu, X. Li, P. Moser, and J.C. van Duysen, Ann. Chim. (Paris) **18**, 287 (1997).

[6] P. Hohenberg and W. Kohn, Phys. Rev. B **136**, 864 (1964); W. Kohn and L. Sham, *ibid.* **140**, 1133 (1965).

[7] J. Hafner, Acta Mater. **48**, 71 (2000).

[8] G. Kresse and J. Hafner, Phys. Rev. B **47**, 558 (1993); **49**, 14 251 (1994).

[9] G. Kresse and J. Furthmüller, Phys. Rev. B **54**, 11 169 (1996).

[10] G. Kresse and J. Furthmüller, Comput. Mater. Sci. **6**, 15 (1996).

[11] D. Vanderbilt, Phys. Rev. B **41**, 7892 (1990); G. Kresse and J. Hafner, J. Phys.: Condens. Matter **6**, 8245 (1996).

[12] J.P. Perdew and A. Zunger, Phys. Rev. B **23**, 5048 (1981).

[13] J.P. Perdew and Y. Wang, Phys. Rev. B **45**, 13 244 (1992).

[14] H.J. Monkhorst and J.D. Pack, Phys. Rev. B **13**, 5188 (1976). In the original Monkhorst-Pack scheme, the k point mesh is always symmetric around the Γ point, whereas very often in our calculations we adopted grids centered at the Γ point.

[15] R.P. Feynman, Phys. Rev. **56**, 340 (1939).

[16] M. Methfessel and A.T. Paxton, Phys. Rev. B **40**, 3616 (1989).

[17] P.E. Blöchl, O. Jepsen, and O.K. Andersen, Phys. Rev. B **49**, 16 223 (1994).

[18] C.S. Becquart, K.M. Decker, C. Domain, J. Ruste, Y. Souffez, J.C. Turbatte, and J.C. van Duysen, Radiat. Eff. Defects Solids **142**, 9 (1997).

[19] M. Ludwig, D. Farkas, D. Pedraza, and S. Schmauder, Modell. Simul. Mater. Sci. Eng. **6**, 19 (1998).

[20] C.S. Becquart, C. Domain, J.C. van Duysen, and J.M. Raulot, J. Nucl. Mater. **294**, 274 (2001).

[21] J.R. Beeler and G.L. Kulcinski, in *Interatomic Potentials and Simulation of Lattice Defects*, edited by P.C. Gehlen, J.R. Beeler, and R.I. Jaffee (Plenum, New York, 1972), pp. 735; C.H. Bennett, in *Diffusion in Solids, Recent Developments*, edited by A.S. Norwick and J.J. Burton (Academic, New York, 1975), pp. 85.

[22] G. Liebfried and N. Breuer, *Point Defects in Metals I*, Springer Tracts in Modern Physics 81 (Springer, Berlin, 1978).

[23] G. Simonelli, R. Pasianot, and E.J. Savino, Phys. Rev. B **50**, 727 (1994).

[24] W.A. Basset and E. Huang, Science **238**, 780 (1987).

[25] S.K. Saxena and L.S. Dubrovinsky, Am. Mineral. **85**, 372 (2000).

[26] D. Andrault, G. Fiquet, T. Charpin, and T. le Bihan, Am. Mineral. **85**, 364 (2000).

[27] W. Schilling, J. Nucl. Mater. **69-70**, 465 (1978).

[28] C. Kittel, *Introduction to Solid State Physics*, 6th ed. (Wiley, New York, 1987).

[29] G. Kresse and D. Joubert, Phys. Rev. B **59**, 1758 (1999).

[30] T. Kraft, P.M. Marcus, and M. Scheffler, Phys. Rev. B **49**, 11 511 (1994).

[31] J. Häglund, Phys. Rev. B **47**, 566 (1993).

[32] G.L. Krasko, Phys. Rev. B **36**, 8565 (1987).

[33] G.L. Krasko and G.B. Olson, J. Appl. Phys. **67**, 4570 (1990).

[34] S.C. Abrahams, L. Guttman, and J.S. Kasper, Phys. Rev. **127**, 2052 (1962).

[35] Y. Tsunoda, J. Phys.: Condens. Matter **1**, 10 427 (1989).

[36] M. Uhl, L.M. Sandratskii, and J. Kubler, J. Magn. Magn. Mater. **103**, 314 (1992).

[37] M. Körling and J. Ergon, Physica B **237-238**, 353 (1997).

[38] H.C. Herper, E. Hoffmann, and P. Entel, Phys. Rev. B **60**, 3839 (1999).

[39] J. Shen, P. Ohresser, Ch.V. Mohan, M. Klaua, J. Barthel, and J. Kirschner, Phys. Rev. Lett. **80**, 1980 (1998).

[40] C.S. Yoo, P. Söderlind, J.A. Moriarty, and A.J. Cambell, Phys. Lett. A **214**, 65 (1996).

[41] M. Acet, H. Zähres, E.F. Wassermann, and W. Pepperhoff, Phys. Rev. B **49**, 6012 (1994).

[42] J. Zhu, X.W. Wang, and S.G. Louie, Phys. Rev. B **45**, 8887 (1992).

[43] W.J. Phythian, A.J. Foreman, C.A. English, J.T. Buswell, M.

Hetherington, K. Roberts, and S. Pizzini, in *Proceedings of the 15th International Symposium on Effects of Radiation on Materials*, edited by R.E. Stoller, A.S. Kumar, and D.S. Gelles (American Society for Testing and Materials, Philadelphia, 1992), p. 131.

[44] T. Kraft, M. Methfessel, M. van Schilfgaarde, and M. Scheffler, Phys. Rev. B **47**, 9862 (1993).

[45] Z.W. Lu, S.H. Wei, and A. Zunger, Phys. Rev. B **41**, 2699 (1990).

[46] J.R. Chelikowsky and M.Y. Chou, Phys. Rev. B **38**, 7966 (1988).

[47] F. Maury, N. Lorenzelli, M.H. Mathon, C.H. de Novion, and P. Lagarde, J. Phys.: Condens. Matter **6**, 569 (1994).

[48] P. Söderlind, L.H. Yang, J.A. Moriarty, and J.M. Wills, Phys. Rev. B **61**, 2579 (2000).

[49] H.E. Schaefer, K. Maier, M. Weller, D. Herlach, A. Seeger, and J. Diehl, Scr. Metall. **11**, 803 (1977).

[50] L. DeSchepper, D. Segers, L. Dorikens-Vanpraet, M. Dorikens, G. Knuyt, L.M. Stals, and P. Moser, Phys. Rev. B **27**, 5257 (1983).

[51] P. Ehrhart, K.H. Robrock, and H.R. Schober, in *Physics of Radiation Effects in Crystals*, edited by R.A. Johnson and A.N. Orlov (Elsevier, Amsterdam, 1986) p. 63.

[52] G. Simonelli, R. Pasianot, and E.J. Savino, in *Materials Theory and Modelling*, edited by J. Broughton, P.D. Bristowe, and J.M. Newsam, Mater. Res. Soc. Symp. Proc. No. 291 (Materials Research Society, Pittsburgh, 1993), p. 567.

[53] P.A. Korzhavyi, I.A. Abrikosov, B. Johansson, A.V. Ruban, and H.L. Skriver, Phys. Rev. B **59**, 11 693 (1999).

[54] W. Frank, U. Breier, C. Elsässer, and M. Fähnle, Phys. Rev. B **48**, 7676 (1993).

[55] A. Vehanen, P. Hautojärvi, J. Johansson, J. Yli-Kauppila, and P. Moser, Phys. Rev. B **25**, 762 (1982).

[56] G.J. Ackland, D.J. Bacon, A.F. Calder, and T. Harry, Philos. Mag. A **75**, 713 (1997).

[57] R.C. Pasianot, A.M. Monti, G. Simonelli, and E.J. Savino, J. Nucl. Mater. **276**, 230 (2000).

[58] G. Simonelli, R. Pasianot, and E.J. Savino, Phys. Status Solidi B **217**, 747 (2000).

[59] Yu. Osetsky, D.J. Bacon, A. Serra, B.N. Singh, and S.I. Golubov, J. Nucl. Mater. **276**, 65 (2000).

[60] H.J. Wollenberger, in *Physical Metallurgy*, edited by R.W. Cahn and P. Haasen, third, revised, and enlarged ed. (Elsevier, Amsterdam, 1983).

[61] F. Ono and H. Mateta, IEEE Transl. J. Magn. Jpn. **6**, 1050 (1991).

[62] M.H. Mathon, Ph.D. thesis, Université de Paris-Sud, 1995.

[63] Q. Chen and Z. Jin, Metall. Trans. A **26**, 417 (1995).

[64] C. Domain, C.S. Becquart, and J.C. van Duysen, in *Microstructural Processes in Irradiated Materials*, edited by G.E Lucas, L. Snead, M. A. Kirk, Jr., and R. G. Elliman, Mater. Res. Soc. Symp. Proc. No. 650 (Materials Research Society, Pittsburgh, 2001), R3.25.

[65] K. Masuda, J. Phys. (France) **43**, 921 (1982).

[66] A. Weidinger, R. Wessner, T. Wichert, and E. Recknagel, Phys. Lett. **72A**, 369 (1979).

[67] G. Brauer and K. Popp, Phys. Status Solidi B **102**, 79 (1987).

[68] A. Möslang, E. Albert, E. Recknagel, and A. Weidinger, Hyperfine Interact. **15/16**, 409 (1983).

[69] F. Maury, A. Lucasson, P. Moser, and F. Faudot, J. Phys.: Condens. Matter **2**, 9291 (1990).

[70] J. Marian (private communication).